IL NUOVO CIMENTO **44 C** (2021) 60
DOI 10.1393/ncc/i2021-21060-3

COMMUNICATIONS: SIF Congress 2020

Anisotropic ion CSD in ECRIS: Mapping Kα emission and β-decay rates in PANDORA

B. MISHRA(1)(2), A. PIDATELLA(1), S. BIRI(3), A. GALATÀ(4), A. MENGONI(5)(6), E. NASELLI(1)(2), R. RÁCZ(3), G. TORRISI(1) and D. MASCALI(1)

(1) *INFN-LNS - Catania, Italy*
(2) *Dipartimento di Fisica e Astronomia, Università degli Studi di Catania - Catania, Italy*
(3) *Institute for Nuclear Research (ATOMKI) - Debrecen, Hungary*
(4) *INFN-LNL - Legnaro, Italy*
(5) *ENEA - Bologna, Italy*
(6) *INFN, Sezione di Bologna - Bologna, Italy*

received 15 January 2021

Summary. — Interactions between ions and non-homogeneously distributed electrons in a min-B plasma trap result in an anisotropic ion distribution. Since phenomena like Kα X-ray emission and β-decay depend on the ion properties, knowledge of the ion spatial distribution is vital to correlate it with the experimental counterparts of said processes. We present a numerical study connecting electron dynamics with anisotropic ion distribution, based on space-selective ion CSD calculation using a population kinetics code. This was first developed to supplement experimental X-ray imaging plasma diagnostics, but it can now be extended to obtain insights on β-decay rates for the PANDORA_Gr3 (Plasmas for Astrophysics, Nuclear Decay Observations and Radiation for Archaeometry) project as well.

1. – Introduction

Electron Cyclotron Resonance Ion Sources (ECRIS) are versatile devices used to generate and supply highly charged ion beams of variable intensity to high-energy accelerators [1, 2]. These devices are based on the dual concepts of resonance heating using microwaves, and magnetic confinement using a minimum-B structure, which generate a hot plasma composed of multi-charged ions immersed in a dense cloud ($n_e \sim 10^{11\text{–}13}\,\mathrm{cm}^{-3}$) of energetic electrons ($k_B T_e \sim 0.1$–$100\,\mathrm{keV}$), remaining stable enough for several hours or days [3-6]. The PANDORA_Gr3 project is a new facility proposed at INFN-LNS which aims to exploit these properties for interdisciplinary research in nuclear astrophysics, plasma physics and material sciences [8]. Among the many phenomena that can be studied in plasma, nuclear β-decay is of significant importance. Accurate data on the half-lives ($t_{1/2}$) of radioisotopes like ^{7}Be and ^{176}Lu are essential inputs for evaluating stellar abundances and solar neutrino fluxes [8]. Interestingly, stellar $t_{1/2}$ can deviate strongly from terrestrially measured values due to the presence of an ionised

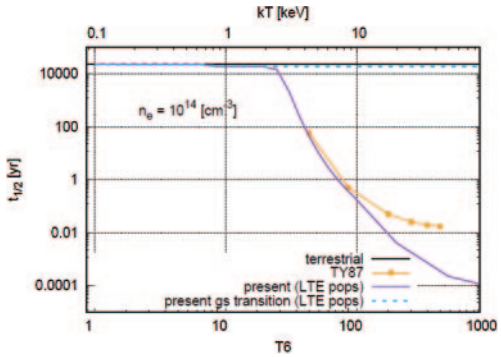

Fig. 1. – $t_{1/2}$ of ^{94}Nb $\longrightarrow$ ^{94}Mo β-decay *vs.* T_e (labelled $T6$ for 10^6 K). *LTE pops* refers to ion population evaluated under local thermodynamic equilibrium, *gs* refers to the ground-state transition and $TY87$ is the data from calculations of Takahashi and Yokoi [7].

environment and this enhancement has been predicted to depend on the charge state distribution (CSD) and level population of the ions in the plasma [9]. These, in turn, are determined by the electron density n_e and temperature T_e, forging a clear connection between in-plasma β-decay modelling and an exhaustive study of ECR plasma dynamics. As an example, we show the estimated variation of $t_{1/2}$ of ^{94}Nb *vs.* T_e and n_e in fig. 1. While the terrestrial values are independent of plasma conditions, transitions to levels beyond the ground state are affected by the environment, significantly altering $t_{1/2}$.

Data from electron dynamics and ion CSD can also be used to simulate plasma X-ray emission, which happens to be a novel diagnostic tool for the PANDORA trap. We thus present here a numerical study of electron dynamics in ECR plasmas, the results of which were used to obtain preliminary ion CSD and Kα emission maps. These can be compared with experimental data for benchmarking the phenomenological models for PANDORA.

2. – Modelling ECR plasmas and electron energy distribution

As a result of minimum-B magnetic confinement and resonance heating, wave-particle energy exchange primarily takes place over a closed and localised surface, labelled B_{ECR} in fig. 2(a). This results in anisotropic energy distribution, further enhanced by the the multimodal nature of the radiation electromagnetic (EM) field. ECR plasma simulations must simultaneously model this spatial anisotropy and wave-particle dynamics, and the LNL and LNS groups achieved this together by developing an iterative routine that self-consistently evolved the EM field with local charge densities in 3D space using COMSOL Multiphysics© as field generator and MATLAB© as particle mover [10]. The outputs were 3D matrices containing electron density $\boldsymbol{\rho}_i$ and energy density $\mathbf{E}_i$ in the intervals $i = (0,2),(2,4),\ldots,(12,\infty)$ keV. The simulation was performed for a microwave frequency 12.84 GHz and power 30 W. The next step was the resolution of the anisotropy to facilitate deduction of the electron energy distribution function (EEDF). This was done by separating the plasma into smaller regions of interest (ROIs), assuming them as containing independent electron populations. We calculated the average electron energy $\langle \mathbf{E} \rangle = \sum_{i=1}^{7} \boldsymbol{\rho}_i \mathbf{E}_i / \sum_{i=1}^{7} \boldsymbol{\rho}_i$, and then grouped together cells which lay in a specific $\langle E \rangle$ range. ROI1 was composed of electrons with $\langle E \rangle = 0$–0.1 keV, ROI2 with $\langle E \rangle = 0.1$–0.2 keV and so on till ROI7 with $\langle E \rangle > 0.6$ keV. Figure 2(b) shows some of these ROIs, and the anisotropy can be appreciated through the shell-like structure where ROIs corresponding to higher energies are located closer to the resonance surface. We then numerically tested several distribution functions to see which of them could most

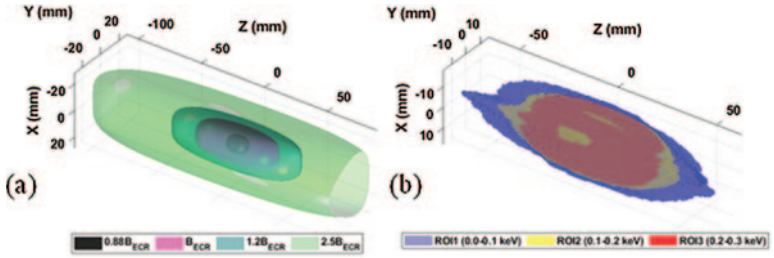

Fig. 2. – (a) Isosurfaces of magnetostatic field and (b) ROIs with different $\langle E \rangle$ (in keV) inside the simulation domain. B_{ECR} is defined according to the resonance condition for angular frequency of the radiation $\omega = eB_{ECR}/m$.

precisely describe the electrons in the energy ranges considered. The goodness of fit of each test EEDF was measured in all the ROIs, using mean squared error (MSE) and r^2 metrics for a comprehensive spatial analysis. Figure 3(a) shows the relative mean MSE of electron density for the tested EEDFs in the different ROIs. We found that a two-component Maxwell+Druyvesteyn (Max+Dr) distribution function of the form

$$(1) \quad f(E, kT_1, kT_2) = N_1 \left(\frac{2}{\sqrt{\pi}} \frac{\sqrt{E}}{\sqrt{(kT_1)^3}} \mathrm{e}^{-E/kT_1} \right) + N_2 \left(1.04 \frac{\sqrt{E}}{\sqrt{(kT_2)^3}} \mathrm{e}^{-0.55E^2/(kT_2)^2} \right)$$

was the best fit to the simulated data, based on the lowest mean MSE, highest mean r^2 and lowest variances almost everywhere. Energies kT_1 and kT_2 lie in the ranges 0–0.1 and 1–10 keV, respectively, and N_1, N_2 are normalisation coefficients. We also noted that deeper in the plasma (ROIs 6 and 7) where there is a sizeable population of energetic electrons, a 3-component Maxwell EEDF works equally well, but no major conclusions about ECR physics can be drawn from this because we are restricted by the energy resolution of our simulated data. For our phenomenological purposes, however, eq. (1) works well enough. Further proof of the usability of the chosen EEDF is clear from the degree of match in fig. 3(b) where we plot collective electron density of some ROIs against that predicted by eq. (1).

3. – Anisotropic ion CSD and Kα emission maps

Using the collective electron density and EEDF parameters of the same ROIs as shown in fig. 3(b), we calculated the probability distribution of the various charge states of ^{94}Nb

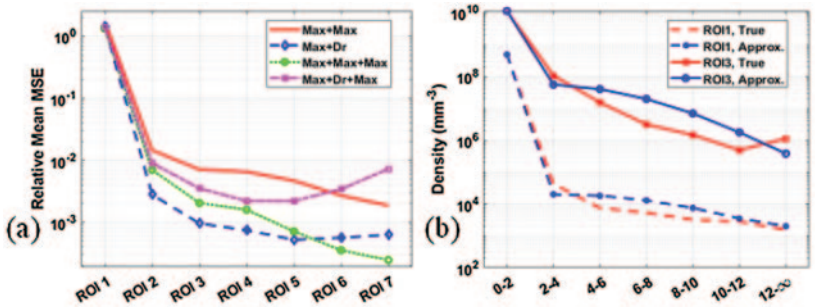

Fig. 3. – (a) MSE averaged over all ROI cells in $(2, \infty)$ keV for different test EEDFs, normalised with n_e^2 and (b) collective density from eq. (1) *vs.* simulations in ROIs 1 and 3.

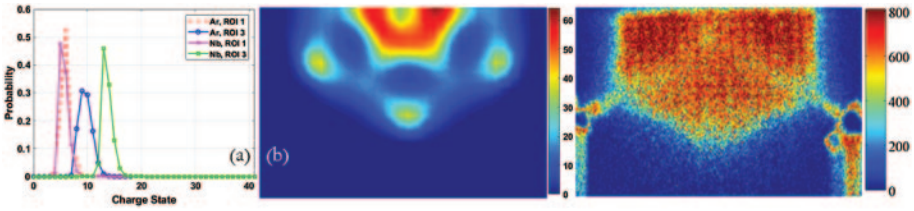

Fig. 4. – (a) Ar and ^{94}Nb CSD in ROIs 1 and 3 and (b) comparison of theoretical (left) and experimental (right) Kα maps [11].

ions embedded in an Ar plasma (fig. 4(a)). As expected, the CSD shifts to higher charge states in ROIs with larger $\langle E \rangle$ because of more energetic electron-ion collisions, and since such ROIs are found deeper in the plasma (fig. 2(b)), the ion CSD in ECR plasmas is highly anisotropic. We also used the $\boldsymbol{\rho}_i$ obtained from numerical simulations with the deduced EEDF to obtain rough Kα emission maps from Ar plasma, and fig. 4(b) shows the comparison between these (left) and experimentally measured (right) maps. The mismatch in photon count distribution is quite obvious, due to a combination of factors like assuming uniform ion charge state, uncertainty in absolute particle density, and neglection of ambipolar diffusion which can cause electron clusterisation in the transverse space and spot-like concentration of photons. Nevertheless, we have been successful in reproducing the emission shape, as well as the "hole" in the near-axis region, which has been observed in other experiments as well. This proves that we are on the right track, and that our models, after due improvements, can reproduce observed emission maps.

4. – Conclusion

We have devised a simple tool to study anisotropic ECR plasma dynamics, and used it to deduce a space-resolved EEDF. By giving the latter as an input to a population kinetics code, we determined plasma ion density and CSD which were used to generate theoretical Kα emission maps. These can be compared with experimental data for benchmarking and further improving the numerical tool. The extracted electron and ion properties will also be used to develop a comprehensive phenomenological model capable of predicting ROI-specific β-decay rates. On this basis, we plan to simulate secondary γ-emission from the decays that can be compared with γ-tagging measurements in PANDORA to validate the model, while also improving the experimental position of detectors.

REFERENCES

[1] Alessi J. G. *et al.*, *Rev. Sci. Instrum.*, **87** (2016) 2.
[2] Se-Yong Choi, Dong-Eon Kim and Volker R. W. Schaa (Editors), *Proceedings of the 22nd International Workshop on ECR Ion Sources (Busan, Korea, 28 August - 1 September 2016)* (CERN) 2017, `https://accelconf.web.cern.ch/ecris2016`.
[3] Leitner D. and Lyneis C. M., *ECR Ion Sources*, in *The Physics and Technology of Ion Sources*, edited by Brown Ian G. (Wiley and Sons) 2004, chapt. 11.
[4] Gott Yu. V. *et al.*, *Nucl. Fusion Suppl.*, **Part 3** (1962) 3 1045.
[5] Stix T. H., *Waves in Plasmas* (Springer Science and Business Media) 1992.
[6] Geller R., *Electron Cyclotron Resonance and Ion Sources* (IOP Publishing, Bristol) 1996.
[7] Takahashi K. and Yokoi K., *At. Data Nucl. Data Tables*, **36** (1987) 375.
[8] Mascali D. *et al.*, *Eur. Phys. J. A*, **53** (2017) 145.
[9] Takahashi K. and Yokoi K., *Nucl. Phys. A*, **404** (1983) 578.
[10] Galatà A. *et al.*, eprint arXiv:1912.01988.
[11] Rácz R. *et al.*, *Plasma Sources Sci. Technol.*, **26** (2017) 075011.